

Multiferroic Dark Excitonic Mott Insulator in the Breathing-Kagome Lattice Material Nb_3Cl_8

Mahtab A. Khan

*NanoScience Technology Center, University of Central Florida, Orlando, FL USA and
Department of Physics, Federal Urdu University of Arts, Sciences and Technology, Islamabad, Pakistan.*

Naseem Ud Din

Department of Physics, Florida Atlantic University, Boca Raton, FL USA

Dirk Englund

*Department of Electrical Engineering and Computer Science,
Massachusetts Institute of Technology, Cambridge, MA 02139, USA.*

Michael N. Leuenberger

*NanoScience Technology Center, Department of Physics,
College of Optics and Photonics, University of Central Florida, Orlando, FL USA.*

(Dated: December 19, 2024)

Motivated by the recent discovery of flat bands (FBs) in breathing Kagome lattices (BKLs), we present a detailed first-principles study of the optical response of single-layer (SL) Nb_3Cl_8 using the GW-Bethe-Salpeter equation (GW-BSE) method, incorporating self-energy corrections and excitonic effects. Our findings reveal a rich spectrum of strongly bound excitons. The key results are fourfold: (i) SL Nb_3Cl_8 exhibits a dark spin-triplet Frenkel exciton ground state with binding energy substantially larger than the GW-renormalized band gap, giving rise to a negative exciton energy peak at -0.14 eV and indicating an excitonic Mott insulator phase potentially stable at room temperature ($k_B T = 0.025$ eV); (ii) the brightest exciton peak appears at 1.2 eV, in excellent agreement with experimental optical absorption spectra. (iii) We map the low-energy Frenkel exciton system onto a Hubbard model with spin-1 particles on a triangular lattice, resulting in frustrated spin configurations due to antiferromagnetic spin-spin exchange interaction. (iv) As the spin-triplet Frenkel excitons have electric dipoles that interact with each other via electric dipole-dipole interaction, we obtain antiferroelectric ordering, possibly stable at room temperature. Thus, we propose that Nb_3Cl_8 is a multiferroic dark spin-triplet excitonic Mott insulator.

INTRODUCTION

Flat bands (FBs), characterized by nearly constant energy across momentum states, lead to highly localized electronic states with large effective masses and suppressed particle hopping. These FBs foster strong electron correlations and enhanced light-matter interactions, giving rise to novel quantum phenomena. Kagome lattices (KLs), composed of corner-sharing triangles forming a hexagonal structure, can host FBs through geometry and interference-driven electron localization.

The breathing Kagome lattice (BKL), characterized by alternating triangles with unequal bond lengths, observed in Nb halides Nb_3X_8 ¹⁻³ (such as Nb_3Cl_8 , Nb_3I_8 , and Nb_3Br_8 , where Nb atoms form a BKL) introduces a unique geometry that enhances electron localization. In Nb_3Cl_8 , the BKL's network of corner-sharing triangles (see Fig. 1) generates destructive interference in electronic wavefunctions, suppressing kinetic energy and producing dispersionless flat bands (FBs) in momentum space. The breathing distortion breaks inversion symmetry, isolating FBs from dispersive bands and enhancing electron correlations. This suppressed kinetic energy increases Coulomb interactions, enabling exotic quantum phenomena such as strongly bound excitons, magnetism,

and potential topological phases. Remarkably, the flat bands in Nb_3Cl_8 are both distinct and experimentally accessible, in contrast to twisted bilayer semiconductors and traditional Kagome lattices (KLs), where FBs often overlap with a multitude of other bands near the Fermi level or are far away from the Fermi energy, complicating their detection. Moreover, the layered structure of Nb_3Cl_8 allows it to be thinned down to the monolayer limit, further enhancing its appeal and versatility in physical sciences, material science, and engineering.

The Exciton Insulator (EI) phase represents a fascinating quantum state of matter where the Coulomb interaction between electrons and holes drives a spontaneous formation of bound excitonic pairs, leading to a macroscopic condensation^{4,5}. The concept of the excitonic insulator was formally introduced by Jérôme, Rice, and Kohn⁶, who demonstrated that such a phase can emerge in systems with either a small bandgap (narrow-gap semiconductors) or a band overlap (semimetals), where strong electron-hole interactions induce a collective instability. Rice later extended these ideas to discuss the transition between the excitonic insulator and the electron-hole liquid phases, emphasizing the role of density and screening effects in stabilizing these quantum states⁷. Advances in experimental and theoretic

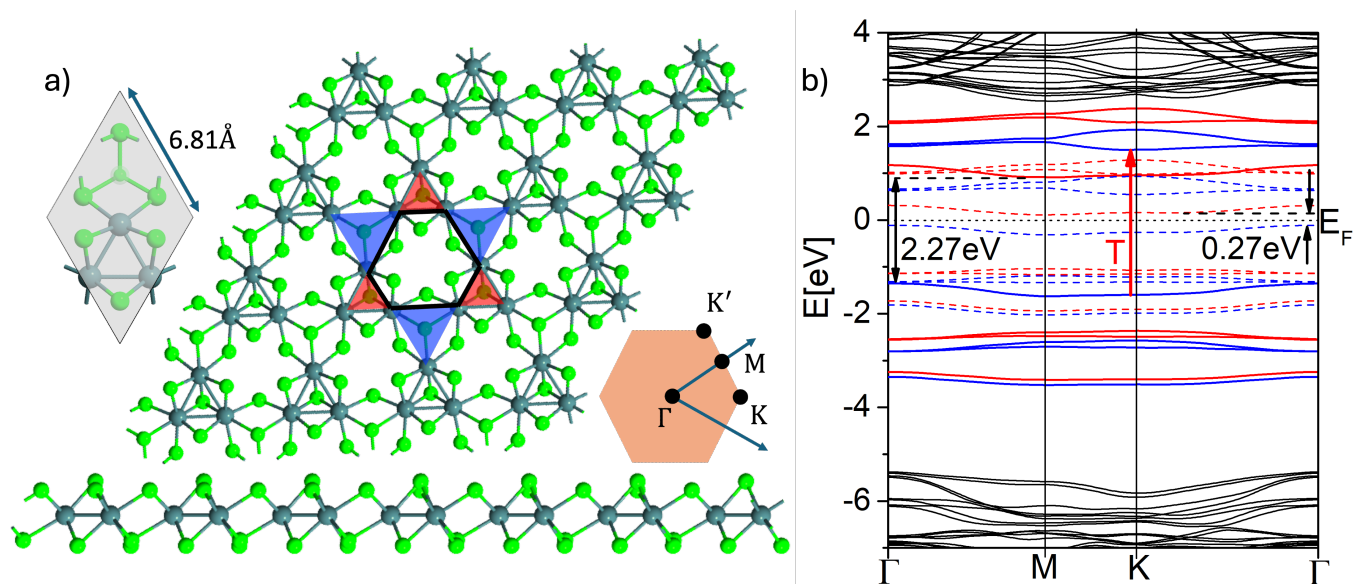


FIG. 1: a) Top and side view of Nb_3Cl_8 , shaded grey (orange) region (rhombus) is the unit cell (Brillouin zone) of Nb_3Cl_8 consisting of 3 Nb (dark green balls) and 8 Cl (light green balls) atoms. Breathing Kagome lattice is formed by Nb atoms creating irregular hexagons (black lines) with two sets of sides of different lengths, resulting in two sets of outer equilateral triangles with different areas (shaded red and blue). SL Nb_3Cl_8 has C_{3v} symmetry. b) PBE (dashed colored curves, blue (red) shows spin-up (down)) $E_g^{\text{PBE}} = 0.27\text{eV}$ and GW (solid blue curves) $E_g^{\text{GW}} = 2.27\text{eV}$ band structure of SL Nb_3Cl_8 , showing substantial increase in the electronic band gap. Black solid lines correspond to the continuum of states.

cal techniques have revealed the signatures of EI phases in materials like transition metal dichalcogenides (e.g., monolayer TiSe_2)^{8,9}, topological insulators¹⁰, and engineered heterostructures¹¹. Recent studies also highlight the interplay between excitonic condensation and other collective phenomena, such as charge density waves and spin-orbit coupling, providing a rich platform for exploring correlated electronic states^{12,13}. These insights are underpinned by first-principles many-body calculations, including the GW-Bethe-Salpeter equation framework, which captures the delicate balance between Coulomb interactions and band structure effects.^{14–22} The EI phase offers exciting prospects for applications in optoelectronics and quantum information, particularly in strongly correlated two-dimensional materials.

Several theoretical studies, including those by Gao et al.²³ and Grytsiuk et al.,²⁴ have described Nb_3Cl_8 as an electronic Mott insulator using single- and multi-orbital Hubbard models, while neglecting excitonic effects, to explain features such as the optical absorption peak at 1.12 eV.¹ These studies assume a metallic phase with half-filled bands at the Fermi level, leading to the emergence of lower and upper Hubbard bands through strong correlation effects.

In stark contrast to previous theoretical studies, our work reveals a fundamentally different perspective on SL Nb_3Cl_8 by using ab-initio Density Functional Theory (DFT) and GW-BSE calculations without any adjustable parameters to calculate its optical response, including

self-energies and excitonic effects. We argue that for SL Nb_3Cl_8 it is necessary to start from the non-collinear DFT result showing exchange interaction-induced band splitting and therefore indicating a semiconductor rather than a metallic phase as the starting point for further calculations. This band splitting invalidates the assumption of a single half-filled band at the Fermi level, challenging the applicability of traditional Hubbard models to this material. Instead, we find that SL Nb_3Cl_8 hosts a large and diverse number of strongly bound excitonic states with novel k-space characteristics not previously seen experimentally or theoretically. Our calculations indicate the presence of a dark exciton ground state at a negative energy $E_{\text{EMI}} = -0.14\text{ eV}$, i.e. being 0.14 eV below the GW-renormalized band gap, with a binding energy of 2.64 eV, providing compelling evidence for an excitonic insulator (EI) phase. To distinguish from exciton condensates,²⁵ we propose that Nb_3Cl_8 exhibits a novel EI insulator phase, namely an Excitonic Mott Insulator (EMI) phase. Furthermore, the brightest exciton peak emerges at $E_{b,\text{max}} = 1.2\text{ eV}$, in excellent agreement with experimental observations¹. Our study provides insight into the electronic structure and flat band-induced excitonic structure in SL Nb_3Cl_8 with a breathing Kagome lattice structure, thereby offering a valuable framework for exploring the interaction between geometry and electron correlations.

I. NUMERICAL RESULTS

a. Electronic Properties: Our model system consists of a single layer (SL) of Nb_3Cl_8 with 11 atoms in the unit cell, where a layer of Nb atoms is sandwiched between layers of Cl atoms, held together through strong covalent bonds as shown in Fig. 1 (a). A breathing Kagome lattice is formed by Nb atoms creating irregular hexagons with two sets of sides of different lengths, resulting in two sets of outer equilateral triangles with different areas, as shown in Fig. 1 (a). The electronic band structure of Nb_3Cl_8 is largely determined by the symmetry properties of the high-symmetry points and lines in the first Brillouin zone of its triangular lattice. Fig. 1 also illustrates both the unit cell and the Brillouin zone of Nb_3Cl_8 . The crystal structure of single-layer (SL) Nb_3Cl_8 exhibits C_{3v} symmetry.

Fig. 1 (b) presents the band structure results from non-collinear SOC calculations, incorporating self-energy corrections through GW (solid curves), alongside PBE results (dashed colored curves). Nearly flat bands with a very small dispersions can be seen, well separated from the continuum of bands and are therefore available for direct experimental observation. A substantial increase of 2 eV in the band gap with the GW correction compared to the PBE highlights the importance of self-energy corrections in Nb_3Cl_8 . In the Supplementary Material, we provide compelling evidence from both unpolarized (UP) and spin-polarized (SP) calculations for the magnetic nature of SL Nb_3Cl_8 . In UP calculations, the electronic states at the Fermi level split in SP DFT, resulting in valence and conduction bands with opposite spin orientations across the Fermi level, which forbids optical transitions from the valence to conduction band, thus leading to the formation of a dark exciton. Interestingly, nonpolarized DFT results indicate that SL Nb_3Cl_8 behaves as a metallic system,^{26,27} highlighting the critical role of spin polarization in accurately capturing the material's magnetic and optical properties. Since we obtain that the 120° spin configuration has the lowest energy, we choose to perform non-collinear DFT calculations. It is interesting to note that flat bands appear in the form of triplets, i.e. a singlet accompanied by a two-fold degenerate doublet. The existence of triplets is a consequence of three-fold rotational symmetry of the crystal.^{28,29}

Since we are interested in the FBs originating from the BKL formed by Nb atoms, we project the FBs in the band structure, onto the d-orbitals of the Nb atoms to investigate the orbital character of the FBs (SI). It can be seen that appreciable d_{z^2} contribution is present in all FBs with conduction and valence bands having the largest contribution. In the analytical modeling section, we develop a single symmetric orbital tight-binding model that corroborates the numerical results, offering further validation and insight into the system's behavior.

b. Optical Properties: Fig. 2 presents the absorption spectra with oscillator strengths for SL Nb_3Cl_8 , both with and without electron-hole interactions. From the os-

illator strength it is evident that the first exciton eigenvalue at $E_{\text{EMI}} = -0.142$ eV is indeed dark. A negative BSE eigenvalue indicates that the ground state exciton possesses an exceptionally large binding energy of 2.64 eV, greater than the material's bandgap. This phenomenon is known as the EI phase,³⁰ where excitonic interactions dominate over free charge carriers. Notably, the BSE ground state corresponds to a dark exciton which couples inefficiently with light. Dark excitons can be populated when a material is cooled, as excitons in higher-energy bright states lose energy and transition to lower-energy dark exciton states. Since the Frenkel excitons are strongly localized on the Nb atoms, we propose a new EI phase for Nb_3Cl_8 called EMI phase.

Although the low-dimensional exciton insulator phase has been proposed in numerous theoretical studies,³⁰⁻³² experimental realization of such systems³⁰⁻³² remains a formidable challenge, demanding precise atomic-scale engineering and control; in contrast, Nb_3Cl_8 has already been successfully realized, marking a significant step forward in this field.

The brightest exciton, the exciton with the highest oscillator strength in BSE susceptibility shown in Fig. 2 (b), has a binding energy of 1.77 eV and lies at an energy of $E_{b,\text{max}} = 1.2$ eV, in excellent agreement with the experimental optical absorption data for SL Nb_3Cl_8 .¹ This alignment with experimental observations underscores the precision and reliability of GW and BSE calculations, affirming their accuracy in capturing the system's optical properties.

c. Optical selection Rules: Nb_3Cl_8 possesses hexagonal symmetry, characterized by a three-fold rotational axis and broken inversion symmetry. Much like a hydrogen atom, an exciton confined to a two-dimensional plane exhibits excitonic angular momentum (EAM) originating from the orbital motion of the electron relative to the hole. Despite inversion-symmetry breaking, we focus on the Γ -point to bypass the need to account for the conservation of valley angular momentum (VAM), which typically arises from broken inversion asymmetry. Additionally, the three-fold rotational symmetry transforms the incoming angular momentum into a modulus of three by absorbing the excess angular momentum into the lattice. Consequently, under normally incident light, the conservation of out-of-plane angular momentum leads to the following optical selection rule:

$$\Delta m\hbar = \Delta l_{ex}\hbar + 3N\hbar \quad (1)$$

Upon photon absorption, the change in momentum, $\Delta m\hbar$, of the incident photon induces a corresponding change in the angular momentum of the exciton, $\Delta l_{ex}\hbar$, and the lattice, quantified as $3N\hbar$, where $N = 0, \pm 1, \pm 2, \dots$. Eq. (1) illustrates the selection rules governing transitions between the d_{z^2} and $\{d_{x^2-y^2}, d_{xy}\}$ orbitals, which require $N = \pm 3$. In contrast, transitions from the orbitals d_{z^2} to d_{yz} and d_{xz} occur when $N = 0$. Notably, out-of-plane transitions between d_{z^2} orbitals are also allowed for $N = 0$. This entire description can be

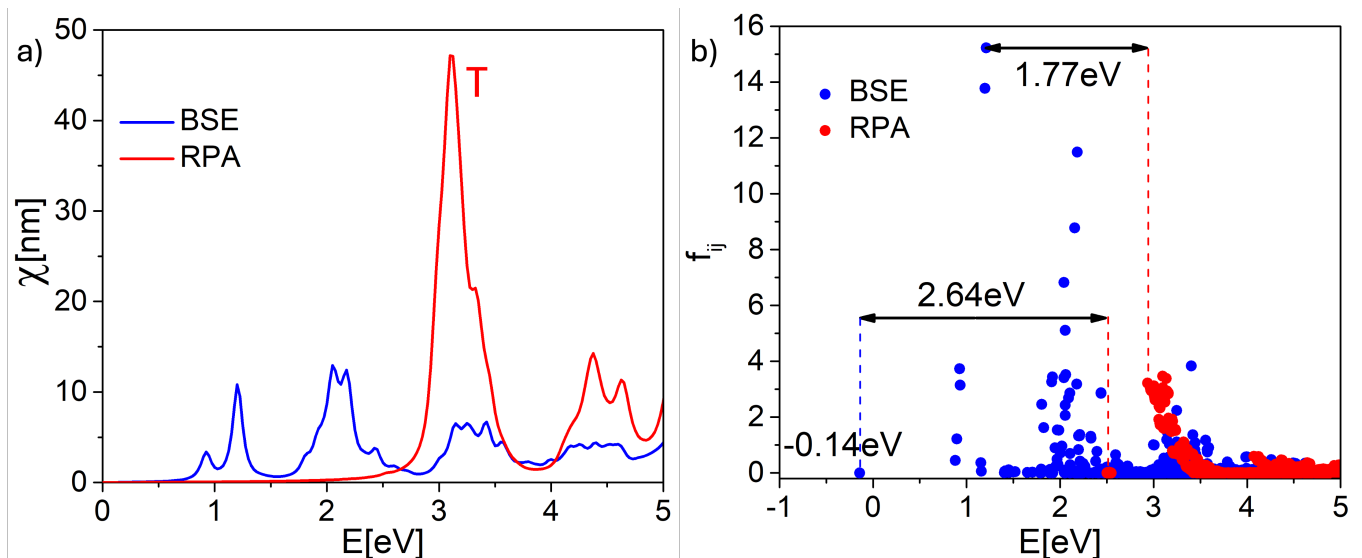


FIG. 2: a) The absorption spectra of SL Nb₃Cl₈, shown without (dashed black curve) and with (solid blue curve) electron-hole interactions, exhibit a prominent peak at 1.2 eV. This peak aligns remarkably well with experimental optical absorption measurements, highlighting the precision of the GW calculations. b) The oscillator strength f_{ij} as a function of energy reveals key insights into the system's excitonic properties. The Bethe-Salpeter Equation (BSE) solution at $E_{\text{EMI}} = -0.14$ eV, which corresponds to the IPA state at 2.5 eV, giving a binding energy of 2.64 eV, $E_{ev} < 0$ exhibits clear signatures of an exciton insulator. In contrast, the first bright exciton, observed at $E_{b,\text{max}} = 1.2$ eV, has a binding energy of 1.77 eV.

rigorously explained using a group-theoretical analysis of the C_{3v} symmetry. Within the electric dipole approximation, transitions between orbitals belonging to different irreducible representations (IRs) are summarized in Table SI in the Supplementary Information. In the electric dipole approximation the optical transitions are governed by the matrix element $\langle \psi_i | x_j | \psi_f \rangle$. The initial state ψ_i , the final state ψ_f , and the position operator x_j transform according to the IRs $\Gamma(\psi_i)$, $\Gamma(\psi_f)$, and $\Gamma(x_j)$, respectively. An electric dipole transition between two states is allowed if the direct product $\Gamma(\psi_i) \otimes \Gamma(x_j) \otimes \Gamma(\psi_f)$ includes $\Gamma(I)$ in its decomposition into a direct sum. Group theoretical description corroborates the selection rules depicted in Eq. (1). Although out-of-plane transitions between the conduction and valence bands are allowed based on orbital character, these transitions are forbidden due to spin selection rules. Fig. 1 illustrates two of the allowed transitions from the valence band (VB) to the doubly degenerate conduction bands CB+1 and CB+2 at the Γ point, which can also be seen as absorption peaks in Fig. 2.

II. RESULTS AND DISCUSSION

A. The Dark Exciton Ground State

Solving the two-band BSE for Nb₃Cl₈, we find that the lowest energy excitonic state is a dark exciton, with an energy of $E_{\text{EMI}} = -0.14$ eV with a binding energy of

2.64 eV. This dark exciton arises from the fact that the conduction and valence bands have opposite spin, forming a spin-triplet exciton state, which effectively doubles the magnetic dipole moment on a trimer from $s = 1/2$ to $S = 1$ when compared with the electronic ground state obtained by DFT only. The exciton wavefunction is centered near the Γ -point in momentum space. The delocalization in \mathbf{k} -space (Fig. 3 (a and b)) indicates a small exciton radius in real space. To estimate its Bohr radius, we calculate the effective masses of the electron and hole in the CB and VB at the Γ -point. We obtain $m_e^* = 2.444m_e$ for the electron and $m_h^* = 2.559m_e$, resulting in an effective reduced mass of $\mu = 1.25m_e$. Thus, for the Bohr radius we obtain $R_B = 1.74$ Å, (for $\epsilon_{\parallel} = 1.818$), indicating localization on a Nb site. Note that the Bohr radius is close to the radius of the Nb atom, which is $R_{\text{Nb}} = 1.46$ Å. Thus, we identify this lowest-energy dark exciton being a Frenkel exciton.

Furthermore, our theoretical analysis of the tight-binding Hamiltonian for a spin-1 particle on a trimer supports these findings. Specifically, we identify the Frenkel exciton to be in the $2a_1$ ground state with orbital angular momentum $m_L = 0$. This state arises from the symmetric combination of the d_{z^2} orbitals of the Nb atoms in the trimer, leading to a localized Frenkel exciton with total spin $S = 1$.

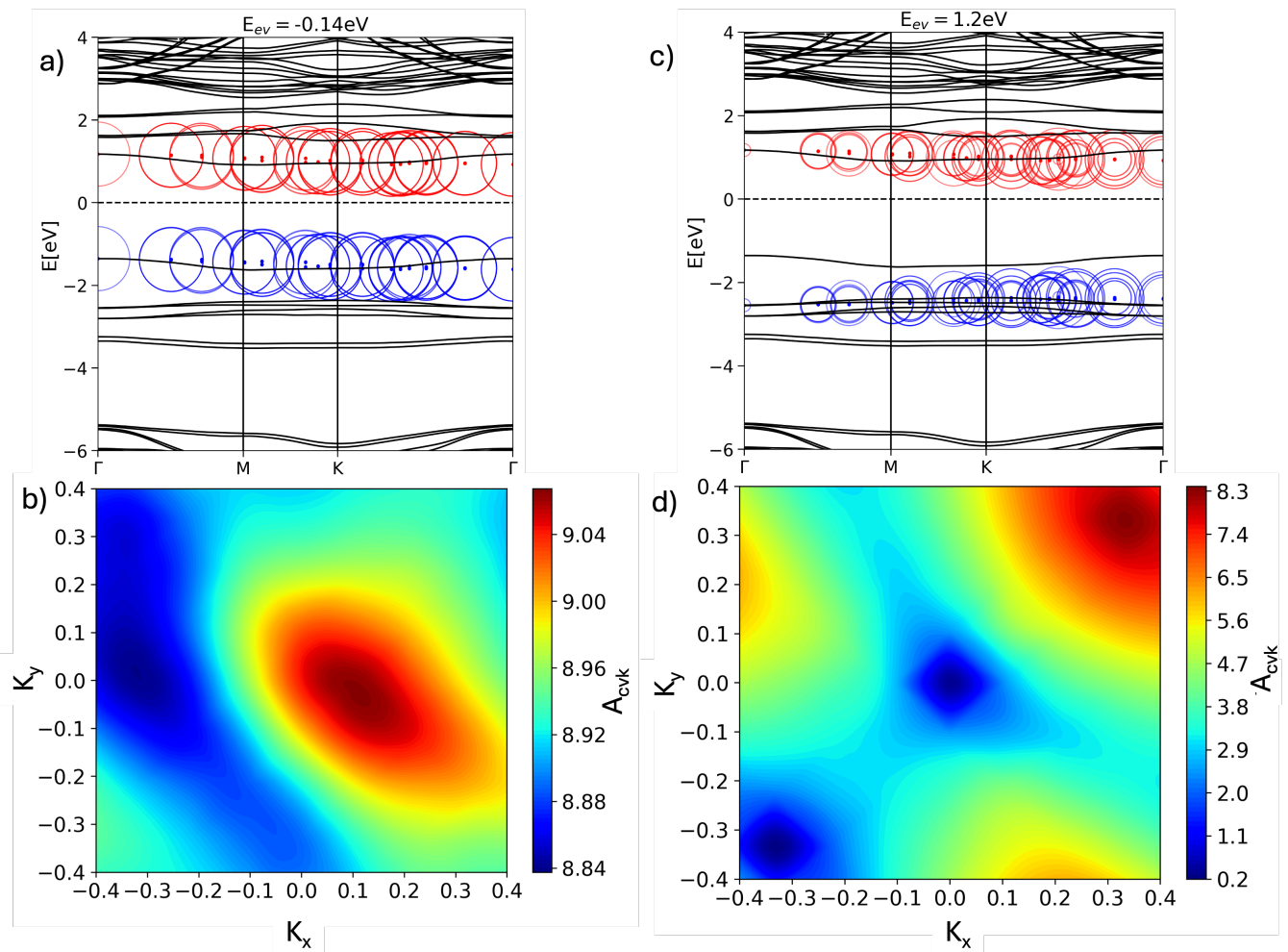


FIG. 3: a) Fat bands obtained for the BSE ground state, corresponding to the eigenvalue of -0.14 eV (dark exciton), are mapped onto the electronic band structure, helping to identify which electron-hole pair contributes most significantly to the BSE eigenstate. Radius of the red (blue) circles show the amplitude of exciton wavefunction. b) The exciton wavefunction amplitude for dark exciton ground state. c) Fat bands are mapped onto the electronic band structure for the dark exciton at an eigenvalue of -0.14 eV. d) The exciton wavefunction amplitude, for the brightest exciton.

B. Magnetic Ordering based on Spin-Triplet Frenkel Exciton

To derive an effective Hubbard Hamiltonian for the spin-1 Frenkel exciton, we note that its binding energy of $E_b = 2.64$ eV is much larger than the intra-trimer hopping energy $t_0 = -0.325$ eV, which is much larger than the inter-trimer hopping energy $t_1 = 0.022$ eV. Since the spin system is based on the single d_{z^2} Nb orbital, for which $m_l = 0$, and, in addition, the molecular orbital $2a_1$ also has $m_L = 0$, we infer that SOC can be neglected, in agreement with previous theoretical studies.²⁴

Therefore, we obtain the effective exchange Hamiltonian

$$H_{\text{eff}} = J \sum_{\langle i,j \rangle} \mathbf{S}_i \cdot \mathbf{S}_j, \quad (2)$$

where J is the exchange coupling between neighboring trimers, \mathbf{S}_i is the spin-1 operator on trimer i , and $\langle i,j \rangle$ denotes neighboring trimers. The exchange coupling J can be estimated in second-order perturbation theory as

$$J = \frac{t_1^2}{U_X} \approx 0.5 \text{ meV}, \quad (3)$$

where $t_1 = 0.022$ eV is the inter-trimer hopping energy, and $U_X \approx 1$ eV is the estimated on-site Hubbard Coulomb repulsion energy for Frenkel excitons in Nb ions.

Since a spin-1 particle on a triangular lattice is expected to behave more classically than a spin-1/2 particle, we propose to use the Weiss mean-field approximation for the spin-1 Frenkel excitons, in which the exchange interaction between neighboring spins can be represented as an effective exchange field acting on each spin. Specifically, each spin experiences a mean field due to its

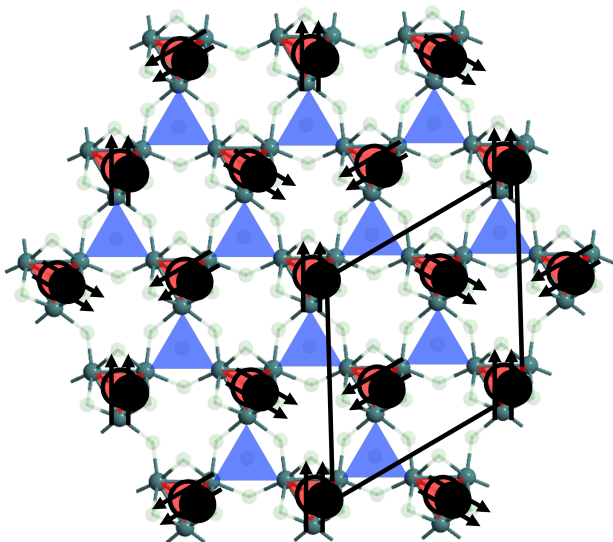


FIG. 4: Each trimer of Nb atoms (dark green balls) has a spin triplet exciton of total spin 1. i.e. both electron (solid black circle) and hole (overlapping empty circle) has parallel in-plane intrinsic spins.

six neighboring spins, which effectively adds a Zeeman-like term to the Hamiltonian. We obtain a 120° spin configuration for the spin-1 Frenkel excitons as the ground state, shown in Fig. 4.

Considering the exchange interaction J and applying the Weiss mean-field theory, the exchange term can be approximated as

$$J \sum_{\langle i,j \rangle} \mathbf{S}_i \cdot \mathbf{S}_j \approx M_{ex} \sum_i S_i, \quad (4)$$

where $M_{ex} = J \sum_{j=1}^6 \langle S_j \rangle = \frac{JzS}{2} = 3J$ is the mean field experienced by the spin-1 particle on each site, $z = 6$ is the coordination number (number of nearest neighbors), and $S = 1$ is the spin of the Frenkel exciton. Compared with the spin-1/2 system on a triangular lattice, the spin-1 system is more stable because the mean exchange field is twice as large. Thus, in the mean-field approximation, the exchange interaction reduces to an effective Zeeman term, which is consistent with the spin splitting between the CB and VB obtained in the spin-DFT and noncollinear DFT calculations.

Our result is in agreement with recent experimental data suggesting antiferromagnetic coupling with a Weiss temperature of $T_W = -18.9$ K or $T_W = -13.1$ K in Nb_3Cl_8 .^{1,33} Its magnitude corresponds to an energy of about $|k_B T_W| = 1$ meV, which is approximately of the order of magnitudes of the estimated values of J and D . The Weiss temperature can be approximated by the formula $k_B T_W = -zJS(S+1)/3$ for a spin- S system.³⁴ Thus, we obtain $k_B T_W = -2J = -1$ meV, in excellent agreement with experimental data.

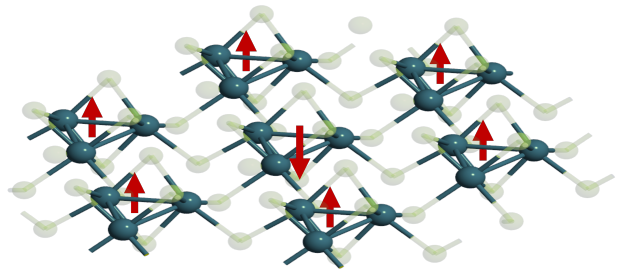


FIG. 5: There is one exciton on each trimer of Nb atoms (dark green balls), which can be considered as an electric dipole pointing out-of-plane, with neighboring dipoles coupled antiferroelectrically.

C. Electric Dipole Ordering based on Spin-Triplet Frenkel Exciton

While in the absence of SOC, spin-triplet excitons are optically inactive (dark) due to spin selection rules, they exhibit an electric dipole moment due to their p-like orbital wave function. Spin triplet excitons are characterized by their total spin quantum number $S = 1$, which arises from the parallel alignment of the electron and hole spins. Since electron and hole are fermions, if the spin part of the exciton is symmetric, the orbital part must be antisymmetric, e.g. p-like.

The spin triplet state comprises three possible spin projections, corresponding to the eigenvalues of the total spin projection operator S_z , i.e. $|S = 1, m_S = +1\rangle = |\uparrow\uparrow\rangle$, $|S = 1, m_S = 0\rangle = \frac{1}{\sqrt{2}}(|\uparrow\downarrow\rangle + |\downarrow\uparrow\rangle)$, and $|S = 1, m_S = -1\rangle = |\downarrow\downarrow\rangle$.

The antisymmetric nature of the spatial wavefunction means the lowest-energy orbital state is p-like, with an angular momentum quantum number $\ell = 1$ and magnetic quantum number $m_L = -1, 0, +1$. Thus, the Frenkel excitons can carry an electric dipole moment due to the separation of the electron and hole. The electric dipole-dipole interaction between two electric dipoles \mathbf{p}_i and \mathbf{p}_j , located at positions \mathbf{r}_i and \mathbf{r}_j , is given by

$$H_{dd} = \frac{1}{4\pi\epsilon_0\epsilon_r} \left[\frac{\mathbf{p}_i \cdot \mathbf{p}_j}{r_{ij}^3} - 3 \frac{(\mathbf{p}_i \cdot \mathbf{r}_{ij})(\mathbf{p}_j \cdot \mathbf{r}_{ij})}{r_{ij}^5} \right], \quad (5)$$

where $\mathbf{r}_{ij} = \mathbf{r}_j - \mathbf{r}_i$ is the displacement vector between the two electric dipoles and $r_{ij} = |\mathbf{r}_{ij}|$ is the distance between them. ϵ_r is the relative permittivity of the material. In the case of Nb_3Cl_8 the dielectric constant exhibits uniaxial anisotropy with the in-plane value estimated by BSE of $\epsilon_{\parallel} = 1.818$ and out-of-plane value of $\epsilon_{\perp} = 1.1285$.

For a triangular lattice, the geometry of the lattice dictates the relative orientations of the dipoles. Similar to the spins, the electric dipoles are also frustrated on a triangular lattice. By comparing the electric dipole-dipole interaction energies $U_{dd,120^\circ} = -95$ meV for 120° in-plane orientation of electric dipoles and $U_{dd,AFE} = -122$ meV for out-of-plane anti-alignment of electric dipoles,

we infer that the electric dipoles of the Frenkel excitons favor the out-of-plane antiferroelectric configuration. The uniaxial anisotropy energy gap can be estimated to be $\Delta_{\text{aniso}} = U_{dd,120^\circ} - U_{dd,\text{AFE}} = 27$ meV, corresponding to a phase transition temperature of $T_{c,\text{AFE}} = 313$ K = 40° Celsius.

D. The Brightest Exciton

The brightest exciton is a bright exciton state with the highest oscillator strength, which occurs at the energy of $E_{\text{brightest}} = 1.2$ eV, with a binding energy of 1.77 eV, corresponding to a spin-singlet exciton. The wavefunction amplitude for this exciton is delocalized in momentum space, with significant contributions from electron-hole pairs near the K-points, reflecting the band structure of the material. The excitonic wavefunctions for the lowest dark exciton and the brightest exciton are shown in Fig. 3.

In stark contrast to previous theoretical studies, where the optical absorption peak at 1.12 eV was attributed to the optical transition between the Hubbard bands related to the $2a_1$ state,^{23,24} our GW-BSE calculation shows that the peak at 1.12 eV is due to the bright exciton that is made of an electron in CB states and a hole in VB-1 and VB-2 states.

III. CONCLUSION

The ab-initio GW-BSE calculation for Nb_3Cl_8 reveals two important features: (i) The lowest-energy exciton is dark due to the spin-triplet configuration of the electron-hole pair. This exciton lies at $E_{\text{dark}} = -0.14$ eV and has a binding energy of 2.64 eV, indicating an exciton insulator state.^{23,33} (ii) The brightest exciton lies at an energy of $E_{\text{brightest}} = 1.2$ eV with a binding energy of 1.77 eV, which is in an excellent agreement with experimental observations.¹

Our ab-initio GW-BSE results redefine the quantum phase of the ground state of Nb_3Cl_8 to be a dark excitonic insulator; more precisely, an excitonic insulator made of Frenkel excitons that are localized on each trimer in the BKL, giving effectively rise to the new quantum phase of excitonic Mott insulator with the Frenkel exciton spin triplets ($S = 1$) arranged in a 120° spin configuration. This result is consistent with experimental data.^{23,33}

Using the classical electric dipole-dipole interaction, we estimate that the electric dipoles of the Frenkel excitons to align in a out-of-plane antiferroelectric configuration with a anisotropy barrier of $\Delta_{\text{aniso}} = 27$ meV, suggesting stability at room temperature.

We predict that the combination of flat bands and electric dipole ordering should give rise to enhancement of second-harmonic generation (SHG), third-harmonic generation (THG), and high-harmonic generation (HHG) in Nb_3Cl_8 , in particular because the antiferroelectric dipole

configuration on a triangular lattice breaks the inversion symmetry. While SL Nb_3Cl_8 should exhibit nonlinear response for all orders n , i.e. nonzero $\chi^{(n)}$ for all integers $n > 2$ due to inversion symmetry breaking, we anticipate that for two and in general an even number of AB-stacked layers of Nb_3Cl_8 the even orders of nonlinear response should vanish, because the inversion symmetry is restored. The reason is that AB stacked (or bulk) Nb_3Cl_8 exhibits D_{3d} point group symmetry,³⁵ which contains the inversion symmetry. Note that bulk Nb_3Cl_8 is typically AB-stacked at room temperature.³⁶

We envision applications in quantum information processing and in neuromorphic machine learning. The excitonic Mott insulating phase of Nb_3Cl_8 at room temperature, coupled with strong second-order nonlinearities ($\chi^{(2)}$), offers a promising route toward robust photonic quantum information processing. Enhanced $\chi^{(2)}/\alpha$ ratios and improved Q -factors, as envisioned by recent theoretical proposals,³⁷ could enable deterministic two-photon gates and the generation of fault-tolerant error-correctable states, including Gottesman-Kitaev-Preskill (GKP) qubits.^{38,39} α denotes the mode coupling loss rate.

Strong $\chi^{(2)}$ -mediated nonlinearities in Nb_3Cl_8 may also benefit photonic machine learning architectures that demand ultrafast and energy-efficient computation. Current coherent optical processors have demonstrated rapid linear algebra operations and reconfigurable interferometric networks.^{40,41} As device losses decrease and Nb_3Cl_8 -based materials achieve higher nonlinear coupling, on-chip nonlinear activation functions and in situ training can be implemented to realize fully integrated optical neural networks.^{42,43}

IV. ACKNOWLEDGMENTS

M. N. L. acknowledges support by the Air Force Office of Scientific Research (AFOSR) under award no. FA9550-23-1-0455 and award no. FA9550-23-1-0472. Calculations were performed at the Stokes high performance computer cluster of the University of Central Florida. The final calculations were performed on the Darwin high performance computer cluster provided by the ACCESS program of the National Science Foundation (NSF). M. N. L. and M. A. K. acknowledge support by the NSF ACCESS program under allocation no. PHY230182 and no. PHY240242.

V. COMPUTATIONAL DETAILS

We consider a unit cell of SL Nb_3Cl_8 , consisting of 11 atoms in a hexagonal structure, with edge lengths $a = b = 6.81$ Å. A vacuum layer of 20 Å is introduced in the z -direction to minimize interactions between the periodic images of Nb_3Cl_8 .

We first perform mean field DFT in generalized gradient approximation (GGA) as implemented in VASP,⁴⁴ on

a $9 \times 9 \times 1$ k-grid with a cut-off energy of 400 eV. For PBE Calculations a band gap of 0.27 eV is obtained Fig. 1 (b) (dashed line). The obtained results are consistent with previous DFT calculations.¹

The GW calculations were initiated using DFT-derived wavefunctions. Self-consistency was achieved by iteratively updating the GW eigen-energies, thereby removing dependence on the single-particle energies obtained from the initial DFT computations. For GW calculations we consider a $9 \times 9 \times 1$ grid with a cut-off energy (ENCUT) of 400 eV. For response function the we set

ENCUTGW=200 eV. The parameter ENCUTGW controls the basis set for the response functions in exactly the same manner as ENCUT for the wave functions. We use 324 empty bands,

Details of the convergence of conduction band, valence band and band gap with respect to the number of bands N_b and number of iterations N_I are shown in the Supplementary Information.

For BSE calculations, we consider 20 bands above and below the Fermi level, it is important to note that results seem to converge at 12 bands above and below the Fermi level.

-
- ¹ Z. Sun, H. Zhou, C. Wang, S. Kumar, D. Geng, S. Yue, X. Han, Y. Haraguchi, K. Shimada, P. Cheng, L. Chen, Y. Shi, K. Wu, S. Meng, and B. Feng, *Nano Letters* **22**, 4596 (2022).
 - ² S. Regmi, T. Fernando, Y. Zhao, A. P. Sakhya, G. Dhakal, I. Bin Elius, H. Vazquez, J. D. Denlinger, J. Yang, J.-H. Chu, *et al.*, *Communications Materials* **3**, 100 (2022).
 - ³ S. Regmi, A. P. Sakhya, T. Fernando, Y. Zhao, D. Jeff, M. Sprague, F. Gonzalez, I. Bin Elius, M. I. Mondal, N. Valadez, D. Jarrett, A. Agosto, J. Yang, J.-H. Chu, S. I. Khondaker, X. Xu, T. Cao, and M. Neupane, *Phys. Rev. B* **108**, L121404 (2023).
 - ⁴ N. F. Mott, *Philosophical Magazine* (1961).
 - ⁵ L. V. Keldysh and Y. V. KopaeV, *Soviet Physics - Solid State* **6**, 2219 (1968).
 - ⁶ D. Jérôme, T. M. Rice, and W. Kohn, *Physical Review* **158**, 462 (1967).
 - ⁷ T. M. Rice, *Solid State Physics* **32**, 1 (1970).
 - ⁸ H. Cercellier, C. Monney, F. Clerc, C. Battaglia, L. Despont, M. G. Garnier, H. Beck, P. Aebi, L. Pattthey, H. Berger, and L. Forró, *Phys. Rev. Lett.* **99**, 146403 (2007).
 - ⁹ C. Monney, C. Battaglia, H. Cercellier, P. Aebi, and H. Beck, *Phys. Rev. Lett.* **106**, 106404 (2011).
 - ¹⁰ J. Lee, C.-J. Kang, M. J. Eom, J. S. Kim, B. I. Min, and H. W. Yeom, *Phys. Rev. B* **99**, 075408 (2019).
 - ¹¹ M. Fogler, L. Butov, and K. Novoselov, *Nature communications* **5**, 4555 (2014).
 - ¹² A. Kogar, M. S. Rak, S. Vig, A. A. Husain, F. Flicker, Y. I. Joe, L. Venema, G. J. MacDougall, T. C. Chiang, E. Fradkin, *et al.*, *Science* **358**, 1314 (2017).
 - ¹³ D. Varsano, M. Palummo, E. Molinari, and M. Rontani, *Nature nanotechnology* **15**, 367 (2020).
 - ¹⁴ M. S. Hybertsen and S. G. Louie, *Phys. Rev. B* **34**, 5390 (1986).
 - ¹⁵ M. Rohlfing and S. G. Louie, *Phys. Rev. Lett.* **81**, 2312 (1998).
 - ¹⁶ L. X. Benedict, E. L. Shirley, and R. B. Bohn, *Phys. Rev. Lett.* **80**, 4514 (1998).
 - ¹⁷ S. Albrecht, L. Reining, R. Del Sole, and G. Onida, *Phys. Rev. Lett.* **80**, 4510 (1998).
 - ¹⁸ L. Yang, J. Deslippe, C.-H. Park, M. L. Cohen, and S. G. Louie, *Phys. Rev. Lett.* **103**, 186802 (2009).
 - ¹⁹ C. D. Spataru, S. Ismail-Beigi, L. X. Benedict, and S. G. Louie, *Phys. Rev. Lett.* **92**, 077402 (2004).
 - ²⁰ J. Deslippe, C. D. Spataru, D. Prendergast, and S. G. Louie, *Nano letters* **7**, 1626 (2007).
 - ²¹ M. L. C. Steven G. Louie, Elsevier **2**, 1st Edition (2006).
 - ²² A. Steinhoff, M. Rosner, F. Jahnke, T. O. Wehling, and C. Gies, *Nano letters* **14**, 3743 (2014).
 - ²³ S. Gao, S. Zhang, C. Wang, S. Yan, X. Han, X. Ji, W. Tao, J. Liu, T. Wang, S. Yuan, G. Qu, Z. Chen, Y. Zhang, J. Huang, M. Pan, S. Peng, Y. Hu, H. Li, Y. Huang, H. Zhou, S. Meng, L. Yang, Z. Wang, Y. Yao, Z. Chen, M. Shi, H. Ding, H. Yang, K. Jiang, Y. Li, H. Lei, Y. Shi, H. Weng, and T. Qian, *Phys. Rev. X* **13**, 041049 (2023).
 - ²⁴ S. Grytsiuk, M. I. Katsnelson, E. G. C. P. v. Loon, and M. Rösner, *npj Quantum Materials* **9**, 8 (2024).
 - ²⁵ X. Zhu, P. B. Littlewood, M. S. Hybertsen, and T. M. Rice, *Phys. Rev. Lett.* **74**, 1633 (1995).
 - ²⁶ S. Grytsiuk, M. I. Katsnelson, E. G. v. Loon, and M. Rösner, *npj Quantum Materials* **9**, 8 (2024).
 - ²⁷ Y. Huang, S.-S. Gong, and D. N. Sheng, *Phys. Rev. Lett.* **130**, 136003 (2023).
 - ²⁸ M. Erementchouk, M. A. Khan, and M. N. Leuenberger, *Phys. Rev. B* **92**, 121401 (2015).
 - ²⁹ M. A. Khan, M. Erementchouk, J. Hendrickson, and M. N. Leuenberger, *Phys. Rev. B* **95**, 245435 (2017).
 - ³⁰ G. Sethi, Y. Zhou, L. Zhu, L. Yang, and F. Liu, *Phys. Rev. Lett.* **126**, 196403 (2021).
 - ³¹ Z. Jiang, W. Lou, Y. Liu, Y. Li, H. Song, K. Chang, W. Duan, and S. Zhang, *Phys. Rev. Lett.* **124**, 166401 (2020).
 - ³² J. Liu, H. Qu, and Y. Li, *arXiv preprint* (2024), [arXiv:2407.13084](https://arxiv.org/abs/2407.13084).
 - ³³ Y. Haraguchi and K. Yoshimura, *Journal of the Physical Society of Japan* **93**, 111002 (2024).
 - ³⁴ S. Mugiraneza and A. M. Hallas, *Communications Physics* **5**, 95 (2022).
 - ³⁵ D. A. Jeff, F. Gonzalez, K. Harrison, Y. Zhao, T. Fernando, S. Regmi, Z. Liu, H. R. Gutierrez, M. Neupane, J. Yang, *et al.*, *2D Materials* **10**, 045030 (2023).
 - ³⁶ J. P. Sheckelton, K. W. Plumb, B. A. Trump, C. L. Broholm, and T. M. McQueen, *Inorg. Chem. Front.* **4**, 481 (2017).
 - ³⁷ S. Krastanov, M. Heuck, J. H. Shapiro, P. Narang, D. R. Englund, and K. Jacobs, *Nature Communications* **12**, 191 (2021).
 - ³⁸ M. Eaton, R. Nehra, and O. Pfister, *New Journal of Physics* **21**, 113034 (2019).
 - ³⁹ K. Takase, K. Fukui, A. Kawasaki, W. Asavanant, M. Endo, J.-i. Yoshikawa, P. van Loock, and A. Furu-

- sawa, *npj Quantum Information* **9**, 98 (2023).
- ⁴⁰ J. Carolan, C. Harrod, C. Sparrow, E. Martín-López, N. J. Russell, J. W. Silverstone, P. J. Shadbolt, N. Matsuda, M. Oguma, M. Itoh, G. D. Marshall, M. G. Thompson, J. C. F. Matthews, T. Hashimoto, J. L. O'Brien, and A. Laing, *Science* **349**, 711 (2015), <https://www.science.org/doi/pdf/10.1126/science.aab3642>.
- ⁴¹ Y. Shen, N. C. Harris, S. Skirlo, M. Prabhu, T. Baehr-Jones, M. Hochberg, X. Sun, S. Zhao, H. Larochelle, D. Englund, and M. Soljačić, *Nature Photonics* **11**, 441 (2017).
- ⁴² X. Lin, Y. Rivenson, N. T. Yardimci, M. Veli, Y. Luo, M. Jarrahi, and A. Ozcan, *Science* **361**, 1004 (2018), <https://www.science.org/doi/pdf/10.1126/science.aat8084>.
- ⁴³ S. Bandyopadhyay, A. Sludds, S. Krastanov, R. Hamerly, N. Harris, D. Bunandar, M. Streshinsky, M. Hochberg, and D. Englund, *Nature Photonics* **18**, 1335 (2024).
- ⁴⁴ VASP, *vasp* **6.3.2** (2022).